nature photonics

ARTICLES

PUBLISHED ONLINE: 12 AUGUST 2012 | DOI: 10.1038/NPHOTON.2012.180

Demonstration of self-seeding in a hard-X-ray free-electron laser

J. Amann[1], W. Berg[2], V. Blank[3], F.-J. Decker[1], Y. Ding[1], P. Emma[4]*, Y. Feng[1], J. Frisch[1], D. Fritz[1], J. Hastings[1], Z. Huang[1], J. Krzywinski[1], R. Lindberg[2], H. Loos[1], A. Lutman[1], H.-D. Nuhn[1], D. Ratner[1], J. Rzepiela[1], D. Shu[2], Yu. Shvyd'ko[2], S. Spampinati[1], S. Stoupin[2], S. Terentyev[3], E. Trakhtenberg[2], D. Walz[1], J. Welch[1], J. Wu[1], A. Zholents[2] and D. Zhu[1]

The Linac Coherent Light Source (LCLS) is an X-ray free-electron laser at the SLAC National Accelerator Laboratory, which has been operating since 2009 for a wide range of scientific research. The free-electron laser process at LCLS is based on self-amplified spontaneous emission (SASE) where spontaneous emission from the initial electron beam shot noise is amplified by its interaction with the electrons over a long magnetic undulator. Although SASE is very effective, producing tremendously powerful, ultrashort X-ray beams, the start-up from noise leaves poor temporal coherence and a broad, noisy spectrum. We present experimental results of a new method, suggested by colleagues at DESY, allowing self-seeding using X-rays from the first half of the undulator to seed the second half through a diamond-based monochromator, producing near Fourier-transform-limited X-ray pulses with 0.4–0.5 eV bandwidth at 8–9 keV. These results demonstrate self-seeding at ångstrom wavelengths with a relative bandwidth reduction of 40–50 with respect to SASE.

X-ray free-electron lasers (FELs), which demonstrate an improvement in peak brightness of approximately ten orders of magnitude over third-generation light sources, have shown remarkable scientific capabilities in biology, chemistry, material science, atomic and molecular physics, as well as many other disciplines. This is exemplified by the successful operation of the Linac Coherent Light Source (LCLS)[1] and SPring-8 Angstrom Compact Free Electron Laser (SACLA)[2]. Other similar X-ray FEL light sources are under construction or development elsewhere in the world. The process of X-ray generation in these machines is based on self-amplified spontaneous emission (SASE)[3,4], where the initial shot noise in the electron beam current produces spontaneous emission that is further amplified by continuous interaction with the electron bunch over the full undulator length, up to the saturation power. The SASE process at LCLS has been quite effective, typically producing tens of gigawatts of tunable X-rays (25–1.2 Å) with pulse lengths as short as 5–10 fs. The X-rays produced in the SASE process are transversely coherent, but the start-up from noise leads to poor temporal coherence with a broad and noisy spectrum. These deficiencies can be corrected if an external seed signal is used to initiate the amplification process; this can result in the production of nearly Fourier-transform-limited X-ray pulses with a much narrower bandwidth than is possible with the SASE process. In addition, seeding can allow a highly efficient undulator field taper to draw even more power from the electron bunch, substantially increasing the photon flux. However, greater benefits from seeding could be derived from the full transverse and temporal coherence of the sub-10 fs X-ray pulses that LCLS will produce.

These radical improvements, on a machine that already represents a revolution in the technology of X-ray production, will be extremely useful to many scientific users pursuing fundamental questions in biology, chemistry, atomic, molecular and materials science, including studies of matter under extreme conditions. The increased spectral brightness will directly impact the performance of specialized X-ray crystal optics, enabling complex pulse manipulation such as pulse split and delay[5], as routinely done with optical lasers. Recent LCLS results[6] indicate that an increased X-ray flux in combination with a reduction in pulse length has the potential to revolutionize the technique of diffraction imaging of biomolecular nanocrystals. In materials science, measuring low-energy excitations under extreme conditions (created either by temperature, pressure or fields) with the high-energy resolution made possible by seeding is critical to the understanding of complex phase transitions in high-temperature superconductors and other novel materials. Unique insights into the dynamics of matter and ultrafast phenomena can also be gained from using ultrashort and temporally coherent X-ray pulses.

A self-seeded FEL

External laser-seeded FELs have been proposed previously for extreme ultraviolet (XUV) and soft X-rays[7,8]. Direct seeding using signals produced in the process of high harmonic generation in gases has been demonstrated in XUV[9]. The first XUV FEL based on high-gain harmonic generation will soon be ready for user operation[10] and will be extended to the soft X-ray wavelength range. However, until very recently, it was envisaged that seeding with ångstrom-scale wavelengths would occur only in the distant future. Because of the difficulty of carrying out external seeding at very short wavelengths, the idea of self-seeding the FEL by using X-rays from the first half of the undulator to seed the second half (Fig. 1) was proposed at DESY for soft X-rays[11] in 1997 and later for hard X-rays[12]; in both cases, the first half of the undulator must operate in the SASE linear regime and the second half should reach FEL saturation. For such a scheme to generate a narrow spectrum, an X-ray monochromator is needed between the first and second

[1]SLAC National Accelerator Laboratory, Stanford, California 94309, USA, [2]Argonne National Laboratory, Argonne, Illinois 60439, USA, [3]Technical Institute for Superhard and Novel Carbon Materials, Troitsk, Russia 142190, [4]Lawrence Berkeley National Laboratory, Berkeley, California 94720, USA.
*e-mail: PEmma@LBL.gov

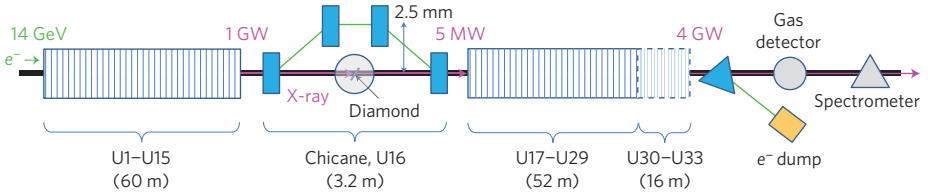

Figure 1 | Layout of the LCLS undulator with a self-seeding chicane, diamond monochromator, gas detector and hard-X-ray spectrometer. The chicane is greatly exaggerated in scale. The last four LCLS undulators (U30–U33) were previously modified as second-harmonic afterburners[15] and were not used in this experiment.

halves, where the FEL power is still low but well above the shot noise power. A typical monochromator (described in refs 10 and 11) has the effect of delaying the X-rays by ~5–10 ps. To match this, the electron bunch must be similarly delayed, requiring a set of strong dipole magnets in a chicane, which are also used to divert the electron beam around the monochromator. These magnets inevitably generate electron energy spread as a result of synchrotron radiation, which can suppress the FEL gain, so an appropriately gentle (long) chicane would not fit conveniently into one short section at X-ray FELs. One way of avoiding the need for this long chicane is to use two separate electron bunches so that the delayed seed from the first bunch will be amplified by the second bunch[13,14].

A more recent hard-X-ray self-seeding scheme[16], again proposed at DESY, consists of using a single diamond crystal in a forward Bragg diffraction (FBD) geometry to produce a temporal waveform of transmitted X-ray pulses with a relatively long monochromatic tail (wake pulse). The properties and underlying physics of FBD relevant to this application are discussed in detail in ref. 17, and briefly in the Supplementary Information. Here, we only highlight that the time dependence t of the radiation envelope of FBD, $G_{00}(t)$ (as shown in Fig. 2c), which represents the crystal response to a very short incident pulse, can be parameterized with the characteristic timescale T_0:

$$\left|G_{00}(t)\right|^2 \propto \left[\frac{1}{T_0}\frac{J_1\left(\sqrt{t/T_0}\right)}{\sqrt{t/T_0}}\right]^2 \qquad (1)$$

where $T_0 = \Lambda^2 \sin\theta/(2\pi^2 cd)$, c is the speed of light, d is the crystal thickness, θ is the X-ray incident angle relative to the crystal atomic planes (Bragg angle), Λ is the extinction length, and J_1 is the Bessel function of the first kind.

Using $d = 0.1$ mm, $\theta = 56.53°$, corresponding to the Bragg reflection condition from the (004) atomic planes of diamond for 8.3 keV photons near the K-edge of nickel, and $\Lambda \approx 22.6$ μm, typical for the 004 reflection, we obtain from equation (1) $t_s = 19$ fs for the location of the first maximum of the monochromatic field with respect to the incident pulse, in good agreement with numeric calculations (Fig. 2). A compact magnetic chicane is then used to delay the electron bunch by this same amount, thus selecting a monochromatic field for seeding. With such a small delay this chicane can fit easily into one 4-m-long space, made available by removal of one of the 33 LCLS undulator sections. The LCLS was recently modified using this approach and the new self-seeding system has been commissioned (Fig. 1).

The existing machine

The LCLS is a hard-X-ray SASE FEL based on the last kilometre of the SLAC linear accelerator. The linac typically accelerates electrons with a single bunch charge between 150 and 250 pC to as high as 15 GeV, with two bunch compressor stages amplifying the peak current to ~3 kA. This high-brightness electron beam is then transported through a 130-m-long magnetic undulator, creating intense transversely coherent hard X-rays with $\sim 2 \times 10^{12}$ photons per pulse at 1.5 Å wavelength (8.3 keV), with a beam repetition rate of 120 Hz. In a special low-charge mode of operation[18] (bunch charge, 20–40 pC), the electron bunch length can be compressed to just 5–10 fs, suitable for self-seeding with the 15-fs-long X-ray wake pulse generated by the diamond monochromator (Fig. 2). The LCLS has now been modified for self-seeding, while preserving the option to quickly switch back to SASE mode (high or low charge) at any time, with no significant loss in FEL performance.

Self-seeding modifications

The self-seeding system (chicane and monochromator) needs to be located at an optimal location along the 130-m-long undulator. The peak X-ray power at the input to the monochromator that is needed to adequately seed the FEL is estimated to be ~1 GW (~10 μJ within a 10 fs pulse length). With normal SASE operation, this power level (in low-charge mode) is typically observed somewhere between undulators U13 and U16 (of 33 undulator sections, each 4 m long). To reliably meet the seed power requirements for the self-seeding experiment, the monochromator and chicane were 'safely' located at U16, which is ~60 m along the undulator line. This choice ensures a seed power that is sufficient for self-seeding to be conclusively tested, although the self-seeding system might eventually be moved upstream by about two undulator sections to improve the seeded performance.

The self-seeding chicane

The 3.2-m-long magnetic chicane installed at U16 includes four dipole magnets, which displace the electrons horizontally by 2.5 mm to bypass the diamond. This also nominally delays the electrons by 20 fs so as to overlap with the delayed monochromatic X-ray seed pulse. Each chicane magnet is 36 cm long, separated from its neighbour by 58 cm, nominally bends the electron beam by ~2.7 mrad with 0.34 T fields, and includes a 576-turn main coil and an independently powered 10-turn trim coil. This allows the chicane to be adjusted between two different configurations: (i) a self-seeded mode, with the electron delay set between zero and 40 fs using the main coils, and (ii) a much weaker 'phase-shift' mode, using the trim coils, with a delay of zero to 10 Å (variable in ~0.04 Å steps). The phase-shift mode (used during SASE operation) allows correction of the electron-to-radiation phase error introduced by the removal of the 4-m-long undulator section at U16. This correction restores the full SASE X-ray pulse energy that was available before the undulator section was removed. In addition, the dependence of the chicane path length on electron energy (given by the R_{56} value of the transport matrix, which is equal to twice the electron delay but expressed in micrometres) washes out the SASE-induced microbunching after the chicane, preparing the electron beam for coherent seeding. With a typical relative electron energy spread of $\sigma_\delta \approx 0.01\%$ r.m.s., the chicane will wash out any temporal structure of wavelength less than $\lambda \approx 2\pi R_{56}\sigma_\delta$ (<80 Å), which is very effective in erasing the 1.5 Å microbunching built up by the 15 undulator sections before the chicane.

The diamond monochromator

The monochromator crystal is a high-quality (see Supplementary Information), 110-μm-thick type-IIa diamond crystal plate, with a

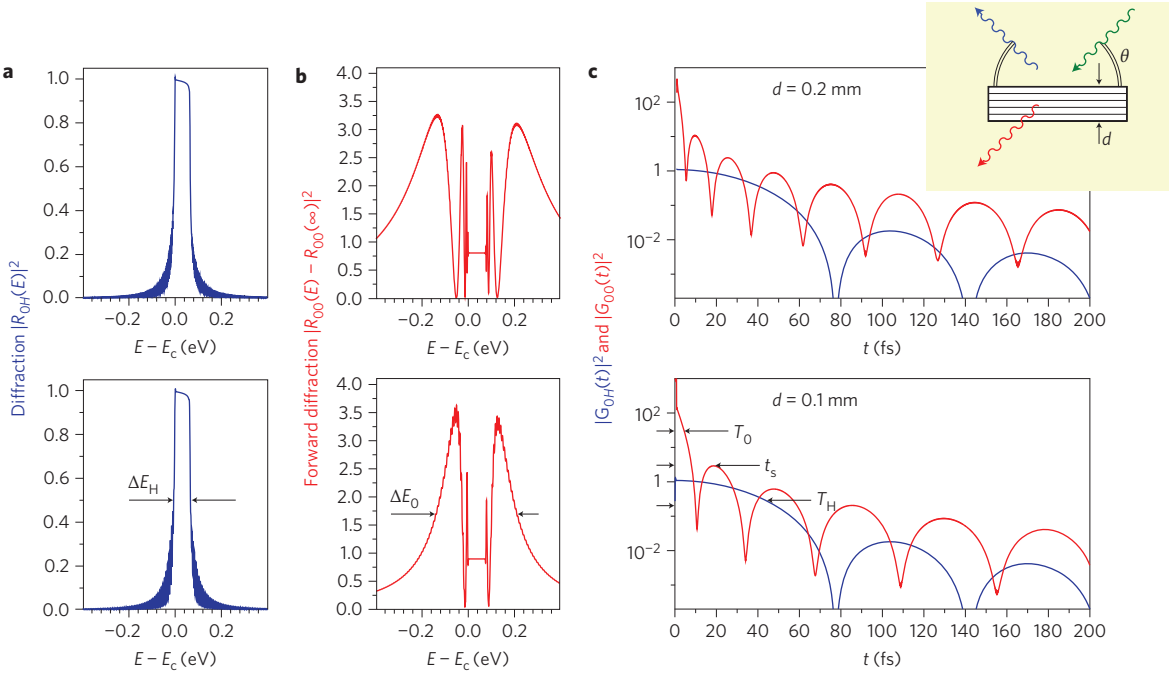

Figure 2 | Spectral and temporal intensity dependences of X-ray Bragg diffraction and FBD. Numerical calculations using dynamical theory of X-ray diffraction for a glancing angle of incidence of $\theta = 56.53^\circ$ to the (004) reflecting atomic planes in diamond, with central X-ray photon energy $E_c = 8.333$ keV. **a**, Spectra of Bragg diffraction $|R_{0H}(E)|^2$ (reflectivity). **b**, Spectra of FBD, with the transmission amplitude far from the Bragg reflection photon energy subtracted. **c**, Time responses $|G_{0X}(t)|^2$ to excitation with a short X-ray pulse in Bragg diffraction ($X = H$, blue) and FBD ($X = 0$, red). Results for diamond crystals with thicknesses $d = 0.1$ and 0.2 mm are shown in the bottom and top plots, respectively.

(004) lattice orientation and a total area of 4.5 mm × 4.0 mm. The diamond crystal was grown from high-purity (99.9995%) graphite at the Technological Institute for Super-hard and Novel Carbon Materials (TISNCM, Troitsk, Russia) using the temperature gradient method under high-pressure (5 GPa) and high-temperature (~1,750 K) conditions. The crystal is installed inside a vacuum vessel, supported gently by a graphite holder, and connected to a remotely controlled, high-resolution rotational stage (Fig. 3) for adjusting the Bragg angle (rotation about the horizontal axis through the middle of the diamond). This is controlled by means of an in-vacuum rotational stage with a range of $\theta = 45$–90° and from the Bragg relation, $\lambda = 2d \sin\theta$, where $d = (3.56712(2)\ \text{Å})/4$ is the spacing between the crystallographic planes for the (004) diamond orientation at 298 K (refs 19,20), allowing for any seed wavelength from ~1.4 to 1.7 Å (12.8–14.2 GeV electrons). Significantly shorter wavelengths are beyond the electron energy reach of the LCLS. Somewhat longer wavelengths would be available using lower-index diamond reflections.

The diamond can also be remotely positioned in the horizontal (x) or vertical (y) directions using two in-vacuum piezo-controlled translation stages. The entire motion control system is mounted on a 10-inch flange with control cable feed-through that bolts to the evacuated monochromator chamber. The monochromator assembly is shown in Fig. 3.

Experimental results and analysis

The LCLS nominally operates at 150–250 pC of charge in a single electron bunch at a repetition rate of 120 Hz. However, the machine can also be run in a low-charge mode[17] where only 20–40 pC of charge is used to generate a much shorter pulse length of 5–10 fs, but with proportionally fewer photons (~0.2×10^{12} photons per pulse at 8 keV). This short pulse provides good overlap with the short seed wake pulse produced by the diamond monochromator and is used for the self-seeded mode of operation. As described above, the low-charge SASE mode of operation produces very limited longitudinal coherence and a broad, noisy photon spectrum with a relative spread of ~0.25% full-width at half-maximum (FWHM; 20 eV). The self-seeded mode is designed to dramatically improve the bandwidth and coherence.

The self-seeded mode is established by inserting the diamond crystal in the SASE X-ray beam path to generate the monochromatic seed pulse, using the chicane to delay the electrons by ~20 fs to overlap the seed. The Bragg angle of the diamond crystal is chosen for the desired seeding wavelength. By adjusting the electron energy, the SASE spectrum produced by the first undulator stage should fully cover this seeding wavelength. The transverse overlap between the seed and the electron beam can be optimized by slightly varying the electron position and angle using the undulator girder position remote control at the beginning of the second undulator stage.

Although up to 15 undulator segments upstream of the seeding section (U1–U15) can be used to generate SASE, which is then 'filtered' by the diamond for seeding, too much SASE radiation actually induces a large growth of the electron energy spread, which then inhibits the gain process for the seeded FEL in the second stage. There is therefore a trade-off between seeding power and seeded FEL gain. Experimentally, we find that using only 13 SASE undulator segments (U3–U15) seems to produce the most seeded FEL power at the end of the LCLS undulator line. The typical SASE pulse energy produced by 13 undulator segments is ~20 μJ with 40 pC of bunch charge.

Another 13 undulator segments (U17–U29) downstream of the seeding section amplify the seeded signal. Figure 4 shows the gas detector signal (X-ray pulse calorimeter), located well after U29, when the chicane is operated in the self-seeding mode. The left side of this time plot is taken when the diamond crystal is retracted from the X-ray beam path, showing a 19 μJ mean SASE background, while the right side is taken when the diamond crystal is inserted, showing a 53 μJ mean seeded FEL signal, including the 19 μJ SASE background. The electron pulse duration at 40 pC was measured to be ~10 fs (FWHM) for SASE operation using a

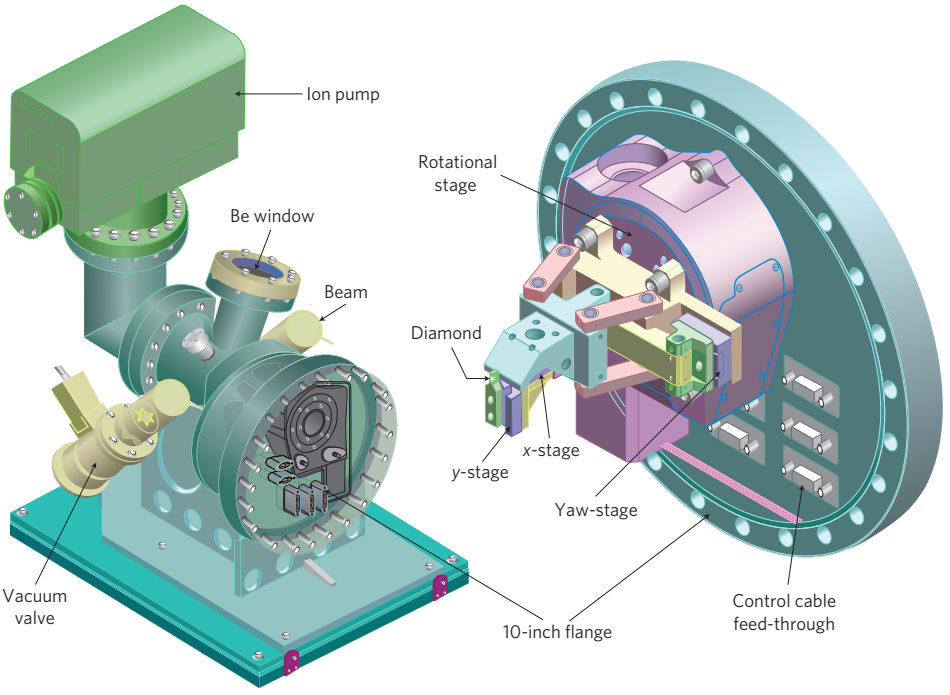

Figure 3 | Monochromator assembly (left) and zoomed 10-inch flange assembly (right). The diamond can be rotated to any Bragg angle from 45 to 90°, with 56.5° as the nominal at 1.5 Å.

longitudinal mapping technique[21]. Assuming the X-ray pulse duration is similar to the electron pulse duration, the average seeded FEL power is ~4 GW and has not reached the saturation level expected at ~10 GW. Because the seed power is generated from the random SASE process and fluctuates close to 100% when a single longitudinal mode is selected, the output FEL energy fluctuates nearly as much for this linear amplifier. In addition, electron energy jitter of 0.05% r.m.s. also contributes significantly to the FEL intensity fluctuation. Peak seeded intensities in excess of 200 μJ have been observed at a bunch charge of 40 pC, but, to date, the variations in shot-to-shot intensity remain larger than 50%.

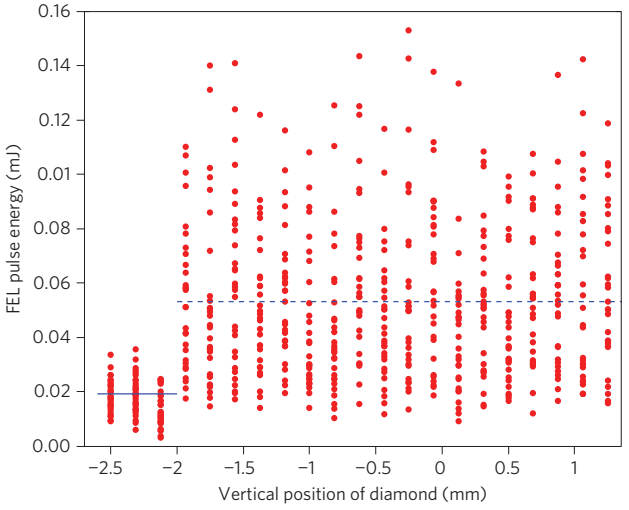

Figure 4 | Each data point is an FEL X-ray pulse total energy measurement made using the gas detector and plotted against the vertical position of the diamond crystal (*y*). The X-ray beam falls off the crystal edge at $y = -2$ mm, showing the SASE background at $y < -2$ mm with a mean pulse energy of 19 μJ (solid blue line). The seeded signal (plus the SASE background) is shown at $y > -2$ mm with a mean energy of 53 μJ (dashed blue line) and peaks at 150 μJ. This does not show the best seeded performance but does reflect the large power fluctuations observed. The chicane is switched on here, which greatly reduces the SASE power from that of normal SASE operation.

Figure 5a shows the single-shot SASE and self-seeded spectra recorded on a Si(333) bent crystal spectrometer[22] with an estimated resolution of 0.1 eV (see Supplementary Information). The SASE spectrum is produced with all 28 undulators, that is, with the chicane off and diamond retracted. In this case, the optimized SASE pulse energy is ~300 μJ with ~20 eV FWHM bandwidth. The seeded signal reaches 240 μJ, and shows a single spectral spike of 0.4 eV (FWHM). The relative FWHM bandwidth is $\sim 5 \times 10^{-5}$ at 8.3 keV, which corresponds to a Fourier-transform-limited X-ray pulse of ~5 fs (FWHM). Figure 5b shows the average SASE spectra for 20,000 shots taken on an Si(111) spectrometer, with a wider range so as to accommodate the electron energy jitter (on the order of 8–10 eV r.m.s.). The FWHM of the average SASE bandwidth is 27 eV without energy jitter correction (as shown) and becomes 20 eV by correcting the electron energy on a shot-by-shot basis. It also shows the average seeded spectra over 200 shots taken on an Si(333) spectrometer under good seeding conditions. The FWHM bandwidth of the average seeded spectrum is ~1 eV. The broadened average bandwidth comes from shot-to-shot spectral variations due to electron energy jitter and other factors. The seeded FEL has a Gaussian spatial mode with excellent transverse coherence.

Start-to-end simulations have been performed using an electron bunch charge of 40 pC, tracking from the photocathode through the accelerator systems, and finally to the FEL undulator. Simulations suggest that 20 μJ SASE radiation produced in the SASE stage (U3–U15) generates sufficient seed power (~5 MW) but degrades the electron beam energy spread. As a result, the FEL signal grows slower in the seeded stage due to increased energy spread and produces 40 μJ FEL pulse energy after 13 undulator segments (U17–U29), without reaching saturation. The simulations also indicate that the seeded FEL spectra are quite sensitive to the detailed longitudinal phase space distribution of the electron beam and suggest further improvements in the seeding performance.

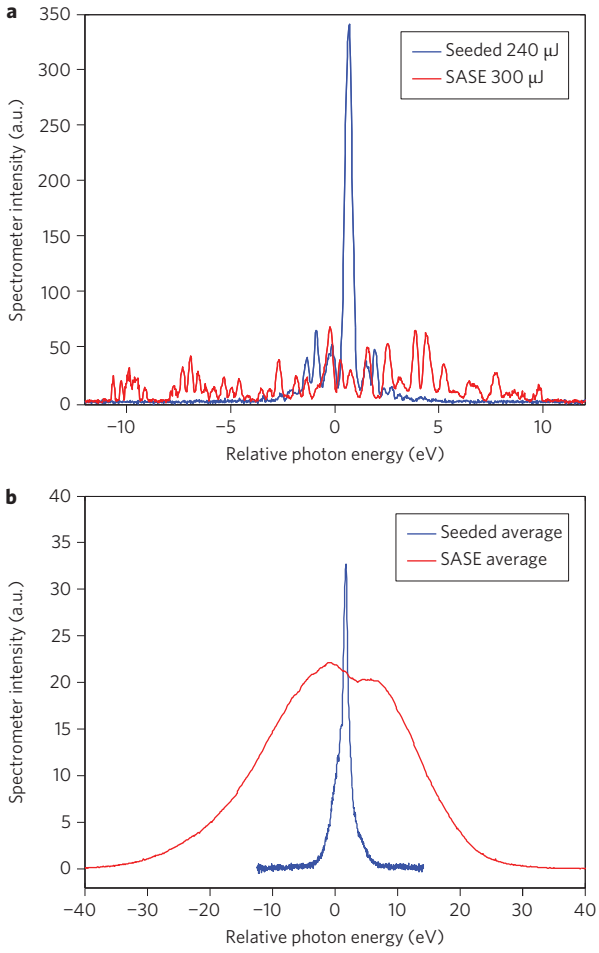

Figure 5 | Measured X-ray spectra. a,**b**, Single-shot (**a**) and averaged (**b**) X-ray spectrum in SASE mode (red) and self-seeded mode (blue). The FWHM single-shot seeded bandwidth is 0.4 eV, whereas the SASE FWHM bandwidth is ~20 eV. Vertical scales have the same arbitrary units in both **a** and **b**. The chicane is turned off for the SASE measurements, but necessarily switched on for the self-seeded mode.

Finally, the chicane strength has also been varied to scan the electron delay so as to trace out the monochromatic wake pulse generated by the diamond crystal. Because the gas detector contains significant SASE background, we use the spectrometer signal and zoom into the narrow-bandwidth seeded spectra for this study. Figure 6 shows the seeded FEL intensity as a function of the chicane delay, reflecting the time dependence of the FBD intensity envelope, in reasonable agreement with FBD theory predictions. The peak seeded signal is reached at a chicane delay of ~19 fs, in agreement with t_s in Fig. 2c (lower). The relatively large error bars for the data (standard deviation) indicate the fluctuating nature of the seeded power, as discussed above.

Summary

FEL self-seeding has been demonstrated at the LCLS using hard X-rays in a low-charge mode of operation. A bandwidth reduction of 40–50 is observed with respect to SASE operation. The SASE bandwidth is ~20 eV (0.25%) FWHM and the single-shot seeded bandwidth is 0.4–0.5 eV FWHM. The stability of the final seeded FEL power is still poor (~50% r.m.s. fluctuations), due in part to shot-to-shot electron energy variations, but also due to the lack of FEL saturation in the seeded half of the undulator. Since the experiment, the last four undulator sections have been added back into the LCLS at slots U30–U33 (second-harmonic undulators were

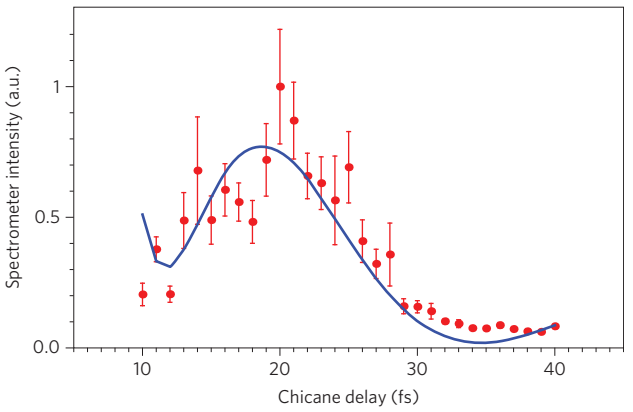

Figure 6 | Seeded FEL intensity as a function of chicane delay, measured using the intensity of just the narrow seeded line on the X-ray spectrometer. The points are the spectrometer signal and the solid curve is the convolution of the diffraction theory prediction of equation (1) with X-ray pulse duration. Crystal thickness and X-ray pulse duration are taken to be fitting parameters. The best fit is obtained when $d = 104$ μm with a flat-top X-ray profile of 5.5 fs.

installed in these slots over the previous year for a separate experiment). Future plans include achieving saturation in the seeded FEL with these four additional undulators, possibly by relocating the chicane and monochromator assembly upstream by about two 4-m-long undulator sections. In addition, a 150-μm-thick diamond crystal producing an approximately twofold more powerful monochromatic wake may also be tested. In the longer term, more undulator sections may be added in order to achieve an aggressive undulator field taper to enhance the seeded FEL power by perhaps another order of magnitude. Such FEL development may eventually lead to obtaining fully coherent, transform-limited, ultrashort hard-X-ray pulses with terawatt power levels[23].

Received 26 March 2012; accepted 29 June 2012;
published online 12 August 2012

References

1. Emma, P. *et al.* First lasing and operation of an angstrom-wavelength free-electron laser. *Nature Photon.* **4,** 641–647 (2010).
2. Pile, D. First light from SACLA. *Nature Photon.* **5,** 456–457 (2011).
3. Kondratenko, K. & Saldin, E. Generating of coherent radiation by a relativistic electron beam in an undulator. *Part. Accel.* **10,** 207–216 (1980).
4. Bonifacio, R., Pellegrini, C. & Narducci, L. M. Collective instabilities and high-gain regime in a free electron laser. *Opt. Commun.* **50,** 373–378 (1984).
5. Roseker *et al.* Performance of a picosecond X-ray delay line unit at 8.39 keV. *Opt. Lett.* **34,** 1768–1779 (2009).
6. Chapman, H. *et al.* Femtosecond X-ray protein nanocrystallography. *Nature* **470,** 73–77 (2011).
7. Yu, L. H. Generation of intense UV radiation by subharmonically seeded single-pass free-electron lasers. *Phys. Rev. A* **44,** 5178–5193 (1991).
8. Stupakov, G. Using the beam-echo effect for generation of short-wavelength radiation. *Phys. Rev. Lett.* **102,** 074801 (2009).
9. Togashi, T. *et al.* Extreme ultraviolet free electron laser seeded with high-order harmonic of Ti:sapphire laser. *Opt. Express* **19,** 317–324 (2011).
10. Allaria, E. *et al.* The FERMI@Elettra free-electron-laser source for coherent X-ray physics: photon properties, beam transport system and applications. *New J. Phys.* **12,** 075002 (2010).
11. Feldhaus, J. *et al.* Possible application of X-ray optical elements for reducing the spectral bandwidth of an X-ray SASE FEL. *Opt. Commun.* **140,** 341–352 (1997).
12. Saldin, E. L., Schneidmiller, E. A., Shvyd'ko, Yu. V. & Yurkov, M. V. X-ray FEL with a meV bandwidth. *Nucl. Instrum. Methods A* **475,** 357–362 (2001).
13. Ding, Y., Huang, Z. & Ruth, R. Two-bunch self-seeding for narrow-bandwidth hard X-ray free electron lasers. *Phys. Rev. ST Accel. Beams* **13,** 060703 (2010).
14. Geloni, G., Kocharyan, V. & Saldin, E. Scheme for generation of highly monochromatic X-rays from a baseline XFEL undulator. DESY 10-033 (2010).
15. Nuhn, H.-D. *et al.* Characterization of second harmonic afterburner radiation at the LCLS. *Proc. FEL Conf. 2010* 690–695 (2010).

16. Geloni, G., Kocharyan, V. & Saldin, E. A novel self-seeding scheme for hard X-ray FELs. *J. Mod. Opt.* **58,** 1391–1403 (2011).
17. Lindberg, R. & Shvydko, Yu. Time dependence of Bragg forward scattering and self-seeding of hard X-ray free-electron lasers. *Phys. Rev. ST Accel. Beams* **15,** 050706 (2012).
18. Ding, Y. *et al.* Measurements and simulations of ultralow emittance and ultrashort electron beams in the Linac coherent light source. *Phys. Rev. Lett.* **102,** 254801 (2009).
19. Stoupin, S. & Shvyd'ko, Yu. V. Thermal expansion of diamond at low temperatures. *Phys. Rev. Lett.* **104,** 085901 (2010).
20. Stoupin, S. & Shvyd'ko, Yu. V. Ultraprecise studies of the thermal expansion coefficient of diamond using backscattering X-ray diffraction. *Phys. Rev. B* **83,** 104102 (2011).
21. Huang, Z. *et al.* Measurement of femtosecond LCLS bunches using the SLAC A-line spectrometer. *Proc. Part. Accel. Conf. 2011* 2459–2461 (2011).
22. Zhu, D. *et al.* A single-shot transmissive spectrometer for hard X-ray free electron lasers. *Appl. Phys. Lett.* **101,** 034103 (2012).
23. Fawley, W. *et al.* Towards TW-level LCLS radiation pulses. *Proc. FEL Conf. 2011* paper TUOA4 (2011).

Acknowledgements

The authors would like to thank the SLAC controls, alignment, operations and engineering groups, and also J. Arthur, A. Brachmann, G. Decker, J. Galayda, P. Den Hartog, N. Holtkamp, J. Quintana, C. Pellegrini, E. Prat, T. Raubenheimer, T. Tanaka, J. Stein, B. Stephenson and L. Young for their support and interest in this work. The authors also thank G. Geloni, V. Kocharyan and E. Saldin for sharing their very effective self-seeding idea and also for participating in its commissioning effort. The authors are grateful for the support of the US Department of Energy, Office of Science (contract no. DE-AC02-76SF00515), and the sponsorship of the LCLS mission by the Office of Basic Energy Sciences. Use of the Advanced Photon Source was supported by the US Department of Energy, Office of Science, Office of Basic Energy Sciences (contract no. DE-AC02-06CH11357). MRCAT operations are supported by the Department of Energy and the MRCAT member institutions.

Author contributions

P.E., J.H., Z.H., R.L., S.St., Y.S. and A.Z. co-wrote the manuscript. V.B. and S.T. developed, tested and provided the diamond crystal. S.St. and Y.S. characterized the diamond. Y.F., D.F., J.H. and D.Z. developed and commissioned the spectrometer. J.K. and A.L. analysed the spectra. D.S. and J.R. designed and tested the monochromator controls. E.T. and D.W. designed and fabricated the chicane magnets and vacuum chambers. V.B., F.-J.D., Y.D., P.E., Y.F., J.F., D.F., J.H., Z.H., J.K., R.L., H.L., A.L., H.-D.N., D.R., J.R., Y.S., S.Sp., S.T., J.W., J.W., A.Z. and D.Z. all performed experiments and analysed data. J.A. and W.B. were the project engineers at SLAC and ANL, respectively, and P.E. and A.Z. were the project physicists, also at SLAC and ANL, respectively.

Additional information

Supplementary information is available in the online version of the paper. Reprints and permission information is available online at http://www.nature.com/reprints. Correspondence and requests for materials should be addressed to P.E.

Competing financial interests

The authors declare no competing financial interests.